An Instrumented Cochlea Model for the Evaluation of Cochlear Implant Electrical Stimulus Spread

Chen Jiang, *Member, IEEE*, Shreya Singhal, Tom Landry, Iwan V. Roberts, Simone R. de Rijk, Tim Brochier, Tobias Goehring, Yu C. Tam, Robert P. Carlyon, George G. Malliaras, and Manohar L. Bance

***Abstract*— Cochlear implants use electrical stimulation of the auditory nerve to restore the sensation of hearing to deaf people. Unfortunately, the stimulation current spreads extensively within the cochlea, resulting in "blurring" of the signal, and hearing that is far from normal. Current spread can be indirectly measured using the implant electrodes for both stimulating and sensing, but this provides incomplete information near the stimulating electrode due to electrode-electrolyte interface effects. Here, we present a 3D-printed "unwrapped" physical cochlea model with integrated sensing wires. We integrate resistors into the walls of the model to simulate current spread through the cochlear bony wall, and "tune" these resistances by calibration with an *in-vivo* electrical measurement from a cochlear implant patient. We then use this model to compare electrical current spread under different stimulation modes including monopolar, bipolar and tripolar configurations. Importantly, a trade-off is observed between stimulation amplitude and current focusing among different stimulation modes. By combining different stimulation modes and changing intracochlear current sinking configurations in the model, we explore this trade-off between stimulation amplitude and focusing further. These results will inform clinical strategies for use in delivering speech signals to cochlear implant patients.**

***Index Terms*—Cochlear implants, electrical stimulus spread, cochlea model, 3D printing**

I. Introduction

COCHLEAR implants (CIs) are considered life-changing devices for the rehabilitation of severe-to-profound hearing loss. CIs consist of an electrode array made of individual electrodes, which are inserted into the cochlea; other relevant components are the case ground electrode (in clinical implantation typically located underneath the temporal muscle), and the internal/external receiver and stimulating package (Fig. S1). They function by transforming acoustic sounds into electrical signals that directly stimulate the auditory nerve, instead of via the damaged sensory hair cells. When compared to normal-hearing listeners, CI recipients exhibit poor frequency selectivity and dynamic range [1]. In normal, acoustic hearing, different sound frequencies stimulate different parts of the auditory nerve in a finely grained fashion, as the cochlea is tonotopically organized with higher frequencies represented basally and lower frequencies represented apically. CI stimulation accounts for this tonotopic structure by delivering lower frequency information through apical electrodes and higher frequency information through basal electrodes [2].

While CIs can significantly help people with severe-to-profound hearing loss to regain sound perception, the restored hearing function is far from normal. Most CI users' speech comprehension breaks down in challenging listening conditions with background noise, and music is poorly appreciated [3], [4]. Additionally, a small, but significant proportion of patients perform poorly for speech comprehension even in quiet environments [5]. Despite CIs having up to 26 intracochlear electrodes that can be used for the stimulation [6], traditionally only between 4-8 independent channels of information have been reported [7], [8]. The electrical current injected into the cochlea spreads widely due to the high electrical conductivity of perilymph (the fluid surrounding the electrode array in the cochlea), thereby potentially stimulating a wide region of the auditory nerve [9]. This current spread causes perceptual overlap between the signals on different stimulating electrodes and results in "blurring" of the input signal at the neuronal level. 'Blurring' refers to overlap between several stimulated channels and their subsequent interaction, the importance of

This work was supported in part by the Evelyn Trust, the Wellcome Trust Junior Interdisciplinary Fellowship (204845/Z/16/Z), the Cambridge Hearing Trust and in part by Advanced Bionics Corporation for providing cochlear implants and software on this research. The first two authors contributed equally to this work.

C. Jiang, S. R. de Rijk, T. Brochier, I. V. Roberts, and M. L. Bance are with the Cambridge Hearing Group, Department of Clinical Neurosciences, University of Cambridge, Clifford Allbutt Building, Cambridge Biomedical Campus, Cambridge, CB2 0AH, UK (e-mail: mlb59@cam.ac.uk).

S. Singhal and G. G. Malliaras are with Electrical Engineering Division, Department of Engineering, University of Cambridge, 9 JJ Thomson Avenue, Cambridge, CB3 0FA, UK (e-mail: gm603@cam.ac.uk)

T. Landry is with School of Biomedical Engineering, Dalhousie University, 5981 University Avenue, Halifax, NS, B3H 4R2, Canada

T. Goehring and R. P. Carlyon are with the Cambridge Hearing Group, MRC Cognition and Brain Sciences Unit, University of Cambridge, Cambridge, CB2 7EF, UK

Y. C. Tam is with Emmeline Centre, Cambridge University Hospitals Trust, Cambridge, CB2 0QQ, UK

which is seen not just in cochlear implants but also in other neural prostheses that require independent spatial channels for optimal performance, rather than just time domain parameters such as stimulation rate [10], [11]. This is particularly important in damaged cochleae in which there are likely to be regions with missing neural elements (neural "dead regions") in the modiolus, thereby starting out with even further reduced information bandwidth.

Current spread can be manipulated by the stimulation mode, i.e., the relative spatial locations of the current source and the current sink [12]. In the classic monopolar (MP) stimulation mode for devices, the ground is remote and the stimulating electrode is near the neural tissue. In CIs for MP (Fig. 3a), the stimulating electrode is intracochlear and the ground electrode is located on the case of the implant on the side of the head, i.e., outside the cochlea (Fig. S1). MP stimulation generates considerable current spread, as current disperses widely in the cochlea to return to the extra-cochlear ground electrode. To reduce current spread, other grounds using intracochlear CI electrode configurations can be used, such as bipolar (BP) and tripolar (TP) configurations. In BP mode, the current sink is a single intracochlear electrode, and in TP mode, the ground consists of two intracochlear electrodes flanking the stimulating electrode on both sides. Furthermore, variable distances between the stimulating and intracochlear ground electrodes can be configured. Since these BP and TP grounds are closer to the stimulating electrode than in MP mode, they might in principle limit current spreading to undesired parts of the cochlea, and thus improve focusing [2], [13]. However, there is potentially less effective auditory stimulation as the current may be returned to the intracochlear ground electrode(s) without supplying sufficient energy to excite the auditory nerve. To counter this, one method is to use an intermediate degree of current focusing, which can be achieved with BP and TP stimulation modes by moving the current sink electrodes further away from the stimulating electrode instead of using closely-spaced electrodes. In these BP +*n* and TP +*n* stimulation modes, *n* stands for the number of electrodes between the main stimulating electrode and the current sinking electrode(s). Mixtures of these modes can also be used, typically TP with some percentage of the current sunk intracochlearly, and the rest returning to an extracochlear ground on the casing (called partial tripolar (pTP)), and similarly with BP stimulation [14]–[16]. Further research is needed to better understand the effects of current spread by comparing current spread profiles across different stimulation modes. Similar current steering methods are explored in applications of external neural stimulation, for example in the application of current steering in spinal cord stimulation [17].

To understand how stimulation current spreads inside the cochlea, researchers have measured the current spread-induced voltage (SIV) signals *in-vivo* in both humans and animal models using CIs as recording devices [18], [19]. Injecting current on one electrode causes current spread inside the cochlear fluids, and results in a voltage being expressed on other electrodes, which is a function of several parameters, such as the distance from the stimulating electrode, and the impedance to current flow out of the cochlea, both through the walls (transverse impedance) and along the cochlear fluids (longitudinal impedance) [20]. This SIV relative to the ground electrode can be measured and reported in living patients, as CIs are capable of "back telemetry", i.e. reporting measured intracochlear parameters back to interrogating software. These measurements are available in clinical software of some cochlear implant companies, for instance as the trans-impedance matrix (TIM) for Cochlear Corp® devices, impedance field telemetry (IFT) for MEDEL Corp®, or the electrical field imaging (EFI) matrix for Advanced Bionics® devices [21]. In these measurements, CIs are used as both stimulators and recorders. However, these measurements cannot reveal the whole distribution of the SIV in the cochlea. This is because the recorded voltage signal measured from a stimulating electrode contains a considerable voltage component induced at the electrode-tissue/fluid interface, which is unstable over time, and does not reveal the true voltage in the fluid a few micrometers away from the interface. In other words, only the measurements from the non-stimulating electrodes are reliable, as they are measured with essentially no current flow, using high-impedance amplifiers. Hence, there is missing data at the location of the stimulating electrode, which is in fact the most important measurement point to characterize how spatially focused the stimulus is at each electrode. In addition to the *in-vivo* investigations, there have been *in-vitro* studies [19], [22] using these types of measurements, but for which the same problem remains. It is essential to separate the stimulating electrodes and the sensing/recording electrodes to obtain the full distribution of the SIV.

Computational models have been used to predict current spread in the cochlea with different stimulation modes, generally finding that TP and BP mode reduce current spread compared to MP mode. Computational models have been successful in estimating the effect of the spiral cochlea shape on current spread and predicting the neural excitation patterns in response to different modes of stimulation [23]–[33]. Computational models provide some advantages over physical models, including flexibility and the ability to model small anatomical substructures of the cochlea. However, several assumptions and simplifications are made in computational models in order to make the solutions tractable, and physical models are necessary as complements to the computational models. Physical models are able to account for factors which computational models often neglect, including interactions between faradaic and ionic conduction at the electrode/electrolyte interface, and non-linear electrical properties of the actual implanted CI devices as used in practice. Furthermore, the simulation times with computational models scale with the complexity of the models, in contrast to physical, *in-vitro* models, for which measurements can be obtained in real time. Complementary to previous modelling work on CIs, we propose a novel *in-vitro* model approach in this paper, by separating the stimulating and sensing/recording electrodes to obtain the full distribution of the SIV.

In this study, we developed a 3D-printed "unwrapped" artificial cochlea with 14 instrumented sensing electrodes to

measure the SIV signals along the cochlea. By "unwrapped", we mean the snail shape of the cochlea has been reduced to a linear structure, whilst keeping the dimensions and their gradual changes from basal to apical turns similar to those in the human cochlea. Importantly, the voltage measurement locations were placed on the cochlear wall of the stimulated cochlea, and hence occupy a similar location to where the spiral ganglion cells would be in the human cochlea with roughly the same distance between stimulating electrodes and receiving receptors as would occur from electrode to spiral ganglion cells. Furthermore, the recording electrodes do not take up any intracochlear volume, so that the volume of the artificial "perilymph" (in this case saline) is not changed or its electrical characteristics altered. We measured the SIV distribution along the cochlea and compared the SIV distributions under different CI stimulation modes, including MP, BP, TP, and pTP, as well as BP+*n* and TP+*n* modes. The key research questions were: how to optimize a 3D-printed *in-vitro* cochlea model so that it mimics a living cochlea; how the SIV is distributed under different stimulation modes using intra- and/or extracochlear current sinking electrodes; how the different configurations in these stimulation modes affect current spread; and, whether we can find compromises for some trade-offs to potentially optimize CI performance. The ultimate benefit of optimizing a 3D-printed in-vitro cochlea model is the potential ability to rapidly perform studies on multiple types of stimulation strategies and their effects on the electric fields inside the cochlea, without the long processing time required for computational models, and with the complex electrode-electrolyte interface built into the model, which can be difficult to computationally account for.

II. Methods

A. 3D-printed unwrapped cochlea

The 3D model of an unwrapped cochlea (cochlear duct was uncurled to form a linear structure, rather than a complex 3D spiral structure) was designed using Solidworks 2018. The lumen geometry had a circular cross-section with varying diameter along its length according to a previously published measurement of the cross-sectional area in a human cochlea [34] (Fig. 1b). The lumen is tapered with a larger diameter at the base and smaller diameter at the apex (Fig. 1b). The model was 3D printed with clear electrically-insulating methacrylate resin and ultraviolet (UV)-cured using a Formlabs Form 2 3D printer. Note that three scalas were combined together to form the lumen diameter. Teflon coated silver wires (World Precision Instruments AGT1010) were inserted through the model wall every 2 mm, starting 1 mm from the basal opening, and affixed with manually applied UV-cured adhesive (Dymax Multi-Cure 9-911-REV-B). The 2-mm wire spacing was designed to balance the trade-off between the difficulty of close manual wire insertion and density required to reveal SIV distributions. Although the spacing is larger than the electrode spacing of the CI used and so less densely sampling, the wires would record the voltage distributions under different stimulation modes more accurately and precisely, and would actually be more dense sampling than using implant electrodes for pTP+*n* modes, under which the SIV distributions recorded by a CI would be imprecise over 3 mm using Advanced Bionics® devices (of which the electrode pitch is about 1 mm), as several adjacent electrodes are stimulating and cannot record accurately. Wire depths were individually gauged based on a micro-computed tomography scan, and intended to be just at lumen surface level, which was used as an approximation to the voltage measurements at the Rosenthal's canal (where the auditory nerve cell bodies are located in human cochleae). The reasons that Rosenthal's canal was not included were a complete insulation using resin between the Rosenthal's canal and scala tympani would stop current penetrating to the Rosenthal's canal and it was very difficult to create fine porous structures using this 3D printer to allow reasonable current penetration. Teflon coating was used to avoid cross-talk between any two wires when being immersed in saline. The end of the wires facing the cochlea lumen were chlorinated to reduce interface impedance. The apex of the cochlea had a polyethylene tubing with inner diameter of 0.011 inch and outer diameter of 0.024 inch (BD Intramedic PE10), attached with the same UV-cure adhesive as for the wires, to allow saline solution flushing through the cochlea from the apex, while ensuring that no air bubbles were trapped (Fig. S2). We did not include a basilar membrane in our model, as we used only the bony dimensions of the cochlea. Currently, the soft basilar membrane is not possible to replicate in a 3D printed structure. According to previous computational work, a substantial part of the current goes out of cochlea through cranial cavity and scalp [35], [36]; However, in order to reach these routes, current has to escape the cochlear lumen through the bony cochear walls, either modiolar or lateral, before it can flow out of the temporal bone to other portions. The only other routes are through the round window, the cochlear aqueduct, or at the hook region connection to the vestibule, which is also encased in otic bony capsule. In our model, we simplified and combined all the current pathways into the resistors (aside from the inevitable

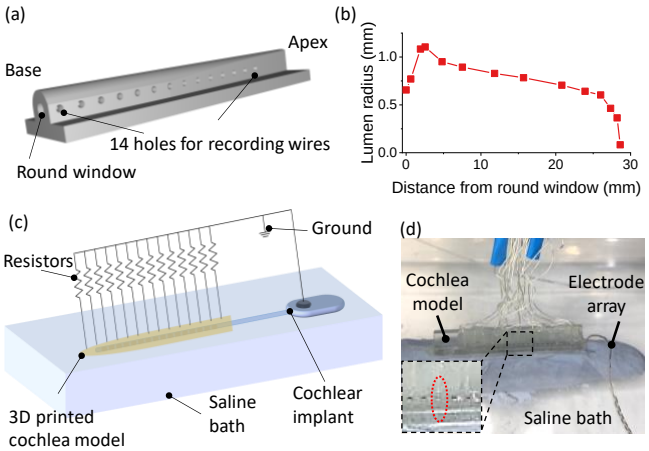

Fig. 1. (a) The 3D schematic model of the 3D-printed unwrapped cochlea. (b) The tapering geometry of the cochlea lumen, with the size of lumen as a function of the distance from the round window. (c) A schematic of the experimental setup for the spread-induced voltage (SIV) measurements. (d) A photo of the CI "implanted" into the 3D printed cochlea model. Inset shows alignment of the 8th electrode (CI) and the 8th wire (cochlea model).

apical and basal fluid channels) in our artifical cochlea model.

B. CI, stimuli and EFI

The HiFocus 1J CI electrode by Advanced Bionics [37] was used in this study. It is a platinum-iridium alloy 16-electrode intracochlear array, housed within a silicone carrier, with an electrode lead fantail extending to the titanium case electronics. The electrodes are embedded on the medial surface of the implant and are numbered 1 to 16 from apex to base. Mapping was done by aligning electrode 8 (CI) and recording wire 8 (artificial cochlea), as shown in Fig. 1d, and scaling the remaining data points according to the relative geometry between the CI and the artificial cochlea wires.

The stimuli were programmed with the Bionic Ear Data Collection System (BEDCS) research software from Advanced Bionics. All the stimulus pulses were charge-balanced, which is ensured by BEDCS, to prevent residual charge that can cause tissue damage [38]. We tested MP, BP, TP and pTP stimulation modes with biphasic pulses, all using 800 μA amplitude stimulation with each phase lasting 32 μs, centered on CI stimulating electrode 8, and aligned visually with the 8th recording wire in the artificial cochlea. These stimulation modes are schematically depicted in Fig. 3a. For the central (8th) electrode of the CI, the pulse was cathodic-leading (Fig. 2a); for the current sinking electrodes, the pulses were anodic-leading (Fig. 3a), and the amplitudes were determined according to the stimulation modes. In MP stimulation, no intracochlear current sinking electrode was used and all the current was sunk to the extracochlear ground electrode. In BP+n stimulations, the pulse amplitude for the intracochlear current sinking electrode was 800 μA. In TP+n stimulations, 400 μA anodic-leading current pulses were sunk to each of the intracochlear current sinking electrodes. For pTP stimulations, σ/2 of the total current pulses were sunk to each of the intracochlear current sinking electrodes, with the remainder (1–σ) sunk to the extracochlear ground electrode. In this study, only the SIV distributions for CI stimulating electrode 8 was presented, which is a representative case for other electrodes and other cochlea models with different geometries and resistances. To provide clinical information specific to a patient, a cochlea model with same geometry and resistivity to that of an individual patient would have to be fabricated and the SIV distributions for each electrode need to be characterised to find how stimulation patterns affect electric fields in that particular cochlea, but we believe we can suggest general findings of interest to all patient geometries.

The EFI was also measured in the artificial cochlea model, using Volta software from Advanced Bionics. The measurement setup was the same as for clinical measurements, i.e., with an amplitude of 32 μA and phase duration of 36 μs. The EFI data in the artificial cochlea model were compared with those obtained from patients. The conduct of this study was approved by the Human Biology Research Ethics Committee, University of Cambridge (Project No. HBREC.2019.42) on 8 January 2020, and by the Research & Development Department, Cambridge University Hospitals NHS Foundation Trust (Project No. A095451) on 11 May 2020.

C. SIV measurement setup

The artificial cochlea lumen was filled with 1% w/v sodium chloride (NaCl) solution, and immersed in a saline bath with the same NaCl concentration. The CI was inserted into the lumen to match the clinically implanted patient scenario (Fig. 2b). The saline filling of the tube was designed to mimic closely the electrical conductivity of the perilymph [39]. The ground electrode from the CI was also immersed in the saline bath. The resistors were grounded to the CI ground electrodes with electrical wires.

The voltage measurements across the resistors were recorded with a Teledyne LeCroy HDO4054A-MS oscilloscope. The sampling rate was 1 GHz. The results were transmitted to a LabVIEW program and conditioned with a digital Butterworth low-pass filter at 6.25 MHz to remove the radio frequency noises from the CI processor. The peak-to-peak voltage between the two phases was extracted as a quantitative measurement for the degree of SIV. The measurements were conducted three times and the standard deviations were calculated. We present the average SIV measurements with standard deviations as error bars. Normalized values were calculated with respect to the highest value recorded. Normalization was used because MP stimulations demonstrated good linearity of SIV growth with stimulus amplitude levels, and similarly with other stimulus modes (Fig. S3).

D. Spread-induced voltage (SIV) signal

To quantify the stimulus spread, we measured the SIV signals (V_{SI}) using the CI to generate current stimuli and the implanted silver wires in the model wall to record the voltage signals, illustrated schematically in Fig. 1c and as photographed in Fig. 1d. We used the BEDCS software from Advanced Bionics to generate a biphasic charge-balanced square wave pulse, delivered by the chosen CI electrode. An example of

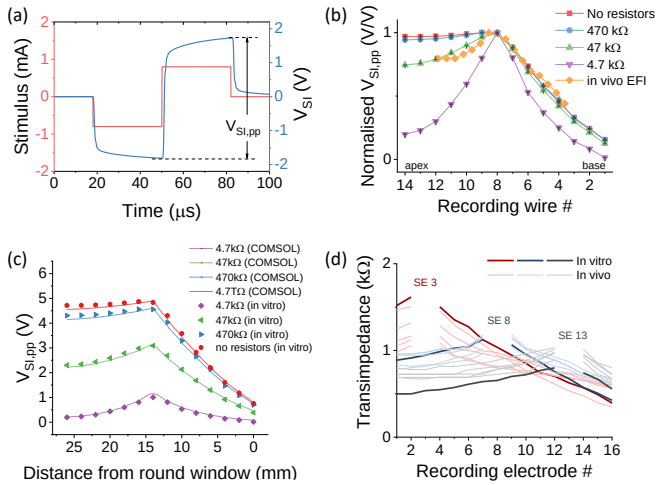

Fig. 2. (a) The current stimulus injected into the cochlea as a function of time and the measured SIV, indicating the peak-to-peak SIV ($V_{SI,pp}$) measured at a recording electrode situated in the model wall. (b) The effect of cross-wall resistors on SIV distribution in the artificial cochlea. The measured $V_{SI,pp}$ was normalised and compared with an *in-vivo* patient EFI profile. (c) The validation of cross-wall resistors by comparing the artificial *in-vitro* model with a computational COMSOL model. (d) The comparison of EFI data between the *in-vitro* model (the average of three measurements) and *in-vivo* patients (collected intra-operatively) under stimulations from electrodes 3, 8 and 13; SE: stimulating electrode.

stimulating and recording is shown in Fig. 2a, where stimulating electrode number 8 and recording wire 8 were used. The measured SIV signal demonstrated a resistor-capacitor circuit like time course, i.e., not a truly square shape. This can be explained by the complex impedance of the saline and the ground electrode, which normally contain both resistance and capacitance components [40], [41]. To measure the degree of spread along the cochlea, we extracted the peak-to-peak voltage ($V_{SI,pp}$) from the measured SIV waveforms at all the recording wires (Fig. 2b). All the $V_{SI,pp}$ data in the main text are shown on a linear scale as with an *in-vitro* study, and the same data presented on a logarithmic scale more related to hearing perception can be found in Fig. S10.

To quantify the stimulation focusing, an exponential decay fitting was used for the normalized SIV data, i.e.,

$$V_{SI,pp}(x) = V_0 + (1 - V_0) * 10^{\pm\frac{\alpha(x-x_0)}{20}} \qquad (2)$$

where V_0 is the baseline level of the SIV, x_0 is where the stimulation is centered, and α is the decay parameter in the unit of decibel per millimeter (dB/mm) (Fig. S4). The sign in the exponent is plus for the fitting at the basal side and minus for the apical side. Such exponential decay fittings are routinely used in other studies [3], [42], [43]. In order to evaluate different stimulation modes, it is important that we used the same criteria to compare them, and so we also used this commonly-used equation. Under tripolar modes, EFI data showed a sharp decrease in the most central electrodes, and these central electrodes are the most influential to the exponential fittings. Therefore, exponential decay fitting parameters could also inform the electrical focusing ability for tripolar modes and other stimulation modes.

We acknowledge that using the SIV signal to estimate the current spread distribution and to describe stimulation focusing is a preliminary approach, since it does not inform us about to neural responses to the stimulation. Neural activation is generally thought to be best predicted by the activation function [24], which is the second derivative of the voltage distribution along the nerve. We are not actually measuring that, but models such as by Kalkman et al [25] imply that having a larger voltage in the cochlea results in greater neuronal activation. In order to understand neural activities in response to stimulation, computational neural models could be used with the SIV data measured in the physical model to try to model voltage patterns along the peripheral processes or central axon. Alternatively, biological neurons can be cultured on the sensing electrodes of the cochlea model, so that neural activities to this SIV signal could be obtained directly. This tool is not completely satisfactory as cultured neurones may not have the same response patterns as "in-situ" spiral ganglion cells. In this study, we focus on the electrical characteristics of the stimulation rather than the resulting neural responses.

III. Results and Discussion

A. 3D-printed cochlea model

The 3D-printed unwrapped artificial cochlea model demonstrated electrical spread characteristics similar to real cochleae. As mentioned above, to simplify the cochlea structure, we 3D-printed an unwrapped artificial cochlea model (Fig. 1a), with a similar geometry to the cochlear lumen in a real cochlea [34] (Fig. 1b). Based on computational modeling, the unwrapped and spiral models appear to have similar electrical spread characteristics (Fig. S13). To simulate the resistance that would normally allow some current to flow out of the cochlear lumen through the bony walls of real cochleae [23], we connected resistors along the length of our artificial unwrapped cochlea connecting the lumen to the surrounding saline bath, in which the casing ground electrode was immersed ("transverse" resistors) since the resin we used for the 3D printed artificial cochlea is not as electrically conductive as real cochlear bone (Fig. 1c). We compared a range of resistance values and "tuned" them to calibrate the electrical characteristics of the artificial cochlea so that we achieved SIV profiles similar to those measured in a typical *in-vivo* patient profile measured using a CI (in this case measured using the EFI function from Advanced Bionics®, as most of our *in-vitro* experiments were also performed with an Advanced Bionics® CI). That is, we aimed to produce the same SIV profile as in real cochlea when measured using the intra-cochlear electrodes in both cases, and then evaluated the voltage spread using our own recording electrodes, which included those placed close to the stimulating electrode. The same resistance values were used for all transverse resistors since in real life, the distances from the recording locations to the remote casing ground electrode are relatively similar, at least in MP mode, with likely the same tissue pathways, and therefore we would expect impedances from the cochlear lumen to the ground to be roughly similar. Therefore, the transverse resistances to ground for MP stimulation are likely to be in the same resistance range but with some variations. We simplified the resistive network and used an identical resistance for all the resistors.

We used the MP mode and biphasic pulses (Fig. 2a) to match our SIV measurements and extracted the peak-to-peak voltage ($V_{SI,pp}$), since this is the configuration used clinically for EFI measurements. Note that a time-dependent increase was observed in the V_{SI} waveform (Fig. 2a), which could be possibly attributed to the capacitive impedance elements in the saline [44] and also saline/wire interface impedances. Despite the real possibility of saline/wire interface impedances confounding measurements, they are likely to be insignificant in impact on the SIV waveforms recorded across the transverse resistors. There are three reasons for this assertion. First, the majority of current flows through the lumen rather than through the sensing wires. At the sensing wire that is closest to the stimulating electrode, the current through that sensing wire and resistor is less than 4% of the total current from the stimulating electrode. Therefore, the saline/wire interface polarisation effect should be small, compared to the effect from the stimulating electrode. Second, the interface impedances are much lower than 47 kΩ transverse resistors (Fig. S14). Therefore, the polarisation voltages induced by the saline/wire interfaces should be much smaller than the voltages across the transverse resistors, and our measurements should approximately reveal the voltages at the lumen. Third, even if the saline/wire interface polarisation potential was significant, it should be negative, i.e., a time-

dependant decrease in SIV waveform rather than an increase as seen in Fig. 2a. This is because, if we assume the polarisation impedance is significant and increases with time, the current flowing through the sensing wires will decrease. Since the resistors have constant resistances, the voltages across the resistors will decrease, which is in conflict to what we measured. For these reasons, we believe the influence from interface impedance to SIV waveform would be insignificant.

The *in-vivo* EFI demonstrated an inverted-V-shaped profile, as depicted in Fig. 2b (see the *x*-axis mapping of *in-vivo* EFI data in Supplementary Materials). Without transverse resistors, the normalized (with respect to the highest value recorded) SIV profile was quite flat at the apical side. This was because, given the insulating resin cochlea wall, there was a more restricted current pathway at the apex of the cochlea than at the base, and therefore the $V_{SI,pp}$ at the apical side was at nearly the same level as at the stimulating electrode. In general, the apical part of the cochlea has a much smaller lumen than the basal side and so there is less conductive electrolyte here for longitudinal charge spread, and EFI or TIM measurements in living subjects generally also show a much flatter SIV at the apical than at the basal end (see 5 *in-vivo* EFI examples in Fig. S7). When transverse resistors were added, the measured SIV starts show an inverted-V-shaped profile, with a more significant decrease in $V_{SI,pp}$ at the basal than at the apical side. Empirically, SIV measurements with 47kΩ transverse resistors demonstrated reasonable agreement with the *in-vivo* EFI. This resistance value is also in the same magnitude range of the transverse resistors from *in-vivo* measurements [21]. Note that using identical resistances for all resistors is not an ideal solution, but it tunes the shape of $V_{SI,pp}$ to match *in-vivo* EFI to a first approximation quite well. Given the fact that *in-vivo* EFI is a result of the combination of individual cochlear geometry and resistivity, it would be impossible to fabricate an *in-vitro* cochlea model that has completely identical EFI to any one individual using just the average human cochlea size and geometry. For future development of *in-vitro* cochlea models, it is essential to obtain linked cochlear geometry information and EFIs from patients. As a simplification, we used 47kΩ resistors in the 3D printed cochlea model to electrically mimic a real cochlea.

To validate the 3D-printed cochlea model, we simulated the model with COMSOL by importing the CAD file used for 3D printing of it, so that theoretically, we have the same geometry design for both 3D-printed *in-vitro* model and computational COMSOL model. As seen in Fig. 2c, the *in-vitro* model and COMSOL model demonstrate similar $V_{SI,pp}$ distribution with different resistor levels. These results also indicate that COMSOL simulation can be used to find the transverse resistances variations to better fit an *in-vivo* EFI, instead of trial and error with different resistances. However, since EFI results from a combination result of cochlea geometry and resistivity, and the cochlea geometry information that linked to the patient was missing, it is not very meaningful to find the exact transverse resistances here without the exact geometry. As an additional validation step, we measured the EFI in the artificial model as well. Despite some higher apical EFI data, the

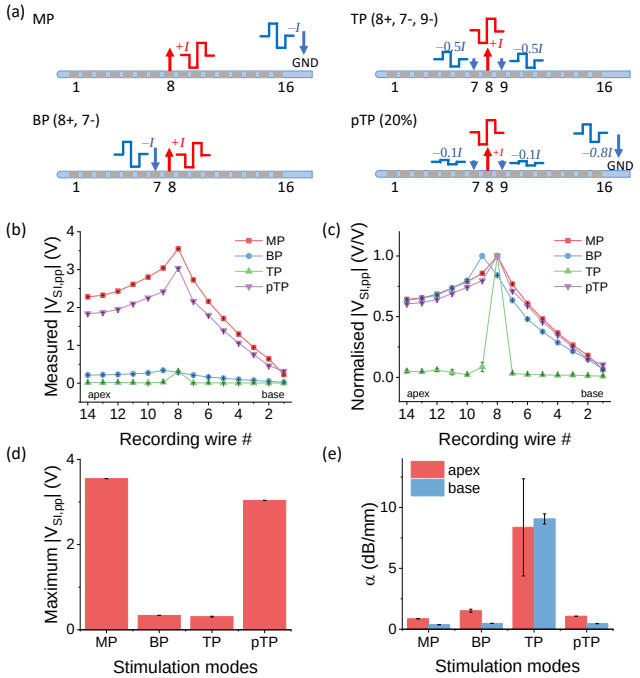

Fig. 3. (a) Schematics of current stimulus injection and sinking under different stimulation modes, namely MP, BP, TP, and pTP. (b, c) The peak-to-peak SIV distribution in the artificial cochlea, (b) as measured and (c) normalised, under different stimulation modes. (d) The maximum absolute measured peak-to-peak SIV and (e) the stimulation focusing under different stimulation modes - an exponential decay fitting was used to extract the decay parameter (α) expressed in units of decibel per millimetre (dB/mm).

artificial model shows a similar EFI profile (the average of three measurements to reduce noises) to *in-vivo* intra-op data (Fig. 2d and S7). The apical EFI profile discrepancy indicates the importance of variations in transverse resistances for future development of artificial models. With COMSOL simulation, we found that the selections of transverse resistances can be optimized to better fit in-vivo EFI data (Fig. S8 and Table S2), with root-mean-square errors below 7%. The combinations of transverse resistances in COMSOL simulation were selected manually and empirically, and can be further optimized and automated using some genetic algorithms or machine learning algorithms. In turn, this will help the design of the transverse resistor network in the in-vitro models.

B. Comparison among classic stimulation modes

We found different stimulation modes demonstrated a trade-off between maximum $V_{SI,pp}$ and stimulation focusing. Again, we are assuming that $V_{SI,pp}$ plays some role in deciding whether a neuron crosses the activation threshold for firing, even though it may not determine the site of activation, which is likely determined by the activation function [24], then the maximum $V_{SI,pp}$ (Fig. 3d) may well be associated with neuronal firing rate [25]. Firing rate and spread would be related to the loudness that CI recipients would perceive (if there were nerve cells in that region), whereas the stimulation focusing is related to the extent of spread of activation among different parts of auditory nerves for a given stimulation electrode, i.e., the bandwidth of the sound. As shown in Fig. 3b-d, MP stimulation mode provided the highest maximum $V_{SI,pp}$ at the 8th recording wire, followed by pTP, BP and TP stimulations. The higher

maximum $V_{SI,pp}$ means that a lower current stimulus amplitude is likely to be needed to achieve the same hearing threshold, and therefore this mode provides the lowest power consumption for a CI. MP stimulation mode does not contain an intracochlear current sinking electrode, so it maximizes the voltage built up between the cochlea and the ground electrode. BP stimulation, by definition, uses one intracochlear current sinking electrode, so that the voltage at the recording site is reduced around this electrode asymmetrically depending on whether the sink electrode is located apical or basal to the stimulating electrode. The sink electrode was pulsed with a biphasic pulse of the opposite polarity to the stimulating electrode. TP stimulation mode used two current sinking electrodes, and therefore the voltage was reduced from both the apical and basal sides of cochlea lumen. Since pTP stimulation can be regarded as a combination of MP and TP stimulations, it demonstrated a maximum $V_{SI,pp}$ between the values obtained from MP and TP stimulation modes.

Note that we also recorded some SIV waveforms in multipolar (BP, TP) stimulation modes with an opposite polarity to the main stimulating electrode, i.e., having an anodic-leading rather than cathodic-leading profile (Fig. S5). This was because we used current sinking electrodes with an opposite polarity in multipolar stimulations, and the voltage induced on the recording electrodes can sometimes be dominated by these current sinks rather than the current source. This has implications for auditory nerve stimulation, especially if there is a larger residual neural population closer to the current sink than the current source, because the auditory nerve is not equally sensitive to anodic and cathodic current [16], [45]–[48]. The details of this are discussed in the Supplementary Materials.

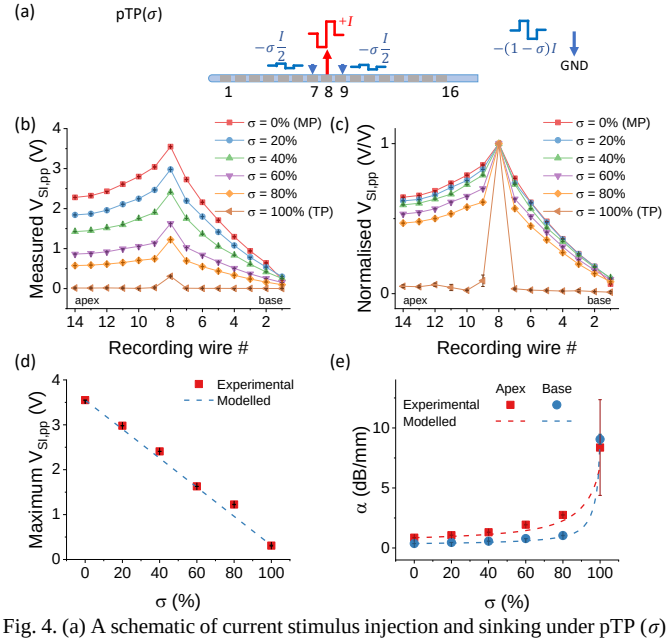

Fig. 4. (a) A schematic of current stimulus injection and sinking under pTP (σ) stimulation. When σ = 0, pTP stimulation mode is MP stimulation by definition, whereas when σ = 100%, it is equivalent to TP stimulation. (b, c) The peak-to-peak SIV distribution in the artificial cochlea, (b) as measured and (c) normalised, under different pTP modes, where σ denotes the percentage of TP mode. (d) The maximum measured peak-to-peak SIV and (e) the stimulation focusing as a function of σ.

In terms of the stimulation focusing, the four stimulation modes showed a reverse trend to their SIV amplitude trend, as shown in Fig. 3e. MP stimulation produced the broadest SIV profile, whereas TP stimulation gave the most focused stimulation. BP stimulation seemed to have a similar focusing effect as MP stimulation, although it was quite asymmetrical (Fig. S6). More discussion about BP stimulations can be found in Supplementary Materials.

The results obtained between different stimulation modes are in good agreement with both analytical and lumped parameter models in the literature [49], [50], with respect to observed trends, apex-to-base profiles and magnitudes. In addition to confirming previous models with actual measurements, we observed some interesting phenomena. Firstly, in both the absolute and normalized results, the current spread towards the apical and basal ends showed an asymmetrical SIV distribution, resulting in a different decaying parameter α on the apical and basal sides. This is likely to be due to the fact that the cochlea lumen at the apical end was essentially sealed by the high-impedance plastic cochlea wall and was much narrower, whereas the basal end is open to the saline bath allowing a clear path for current shunting. This asymmetry is also seen in SIVs in living cochleas (Fig. S7), and so is in keeping with the model representing real cochlear environments. Secondly, although we see increased stimulation focusing in the normalized results in TP versus MP stimulation modes, the absolute results show the maximum $V_{SI,pp}$ with TP stimulation is approximately 10 times smaller than with MP stimulation. If this were reflected in neuronal activation, this would be a problem in terms of power consumption because the electric field needs to exceed a certain threshold for generating neural action potentials and enough for them for sufficient loudness, leading to a trade-off between stimulation focusing and device power consumption.

C. Intra- vs extra-cochlear current sinks in pTP modes

A larger percentage of current sinking to intracochlear electrodes in pTP mode improved stimulation focusing at the cost of a lower maximum $V_{SI,pp}$. Since pTP stimulation is an intermediary between MP and TP stimulation, with a trade-off between maximum $V_{SI,pp}$ and stimulation focusing, we further investigated pTP stimulation to find an optimized pTP trade-off between SIV voltage and focusing. We used σ as the percentage of stimulation current sinking into the intracochlear electrodes and varied the parameter from 0 to 100%.

Assessing the effect of current sinking to intracochlear electrodes by means of varying σ in pTP stimulation (Fig. 4a), the data largely showed similar trends to those previously discussed (Fig. 4b,c). A larger percentage of current sinking to intracochlear electrodes improved the stimulation focusing at the cost of sacrificing the maximum $V_{SI,pp}$. As seen in Fig. 4c, the maximum peak-to-peak SIVs at the 8th recording wire appeared to vary with σ approximately linearly over the range σ = 0% to 100%. According to Wu et al [33], the potential field for pTP mode can be regarded as a linear sum of those from the main and flanking electrodes. This can be described as:

$$V_{SI,pp,pTP}(\sigma, i) = (1-\sigma)V_{SI,pp,MP}(i) + \sigma V_{SI,pp,TP}(i) \quad (1)$$

where $V_{SI,pp,pTP}$, $V_{SI,pp,MP}$ and $V_{SI,pp,TP}$ stand for peak-to-peak SIV

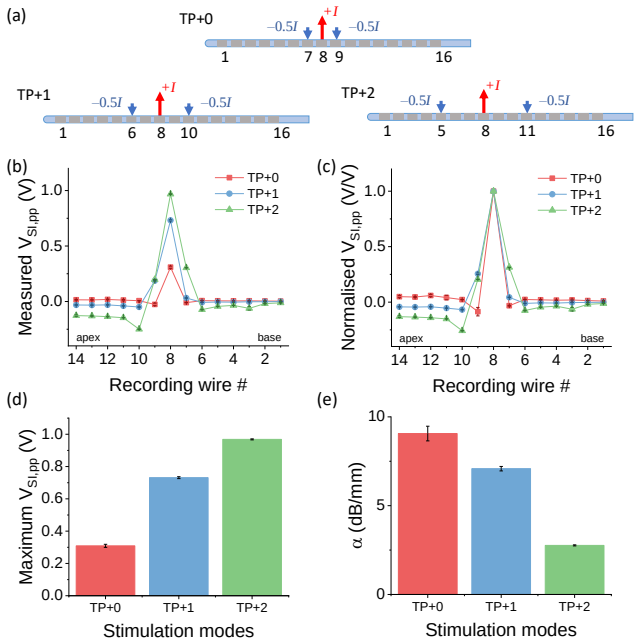

Fig. 5. (a) Schematics of current stimulus injection and sinking under different configurations of TP+*n* stimulation. (b, c) The peak-to-peak SIV distribution in the artificial cochlea, (b) as measured and (c) normalised, under different TP+*n* modes. (d) The maximum measured peak-to-peak SIV and (e) the stimulation focusing under different TP+*n* modes.

amplitude under pTP, MP and TP modes, respectively, at the i^{th} recording wire. From equation 1, which is linear for σ, we modelled the maximum $V_{SI,pp}$ at different σ. As shown in Fig. 4d, the experimental and modelled data were in a good agreement, again confirming that there is good linearity of the measured maximum $V_{SI,pp.}$ However, for the same range, stimulation focusing appeared to be non-linear (Fig. 4e). When σ = 100%, a dramatic increase in the stimulation focusing and reduction in the $V_{SI,pp}$ was measured. For σ = 0% to 80%, there was always some current being drawn towards the extra-cochlear ground, whereas for σ = 100%, the ground was fully intra-cochlear. The confinement of the current pathway to solely intra-cochlear electrodes appeared therefore to have a significant effect on focusing. To understand the dramatic change from σ = 80% to 100%, we modelled the stimulation focusing and extracted the parameter α using equations 1 and 2. As shown in Fig. 4e, the most dramatic change in stimulation focusing happened when σ exceeded 95%.

D. Different current source/sink distances in TP+n modes

Increased intracochlear current sinking electrode distance in TP+*n* stimulation modes decreases power consumption without sacrificing stimulation focusing, where the term +*n* refers to the number of electrodes between the stimulating electrode and current sinking electrode. With regards to the effect of changing distance between stimulating and current sinking electrodes for TP modes (Fig. 5a), our results show that various configurations demonstrated enhanced stimulation focusing, but at the cost of lowered $V_{SI,pp}$ with reducing the distance *n* (Fig. 5b,c). Actually, TP+2 showed a profile that was almost as focused as in TP+0 mode, but with a much higher $V_{SI,pp}$ level (Fig. 5d,e). Comparing with MP mode, the maximum $V_{SI,pp}$ in TP+2 mode was 3.5 times lower, and hence increased power would be needed to match the two modes for stimulating auditory nerves to firing threshold. Despite these power costs, the TP+2 mode has significantly better stimulation focusing when compared to MP mode.

These results support the use of TP stimulation modes with current sinking electrodes further separated than just adjacent to the stimulating electrodes to provide reduced power consumption without sacrificing focusing inordinately. Recommendations between TP+*n* and MP modes will depend on whether the priority is power efficiency or limiting stimulation spread. Whether current spread is still narrower in TP+*n* mode at higher stimulation levels to achieve a similar $V_{SI,pp}$ to MP mode needs to be investigated further, possibly by incorporating a neural model and/or CI patient study.

E. Combining advantages of pTP and TP+n modes

Modelling for pTP+*n* mode shows stimulation amplitude and focusing can be optimized by combining different stimulation modes and changing intracochlear current sinking configurations. Based on the results from TP+*n* and MP modes, we simulated the stimulation levels and focusing abilities in pTP+*n* modes. Here, our hypothesis was that the results in pTP+*n* modes would be a linear combination of TP+*n* and MP modes, for which we found good agreement with the experimental data in pTP stimulation.

In terms of stimulation levels, the maximum $V_{SI,pp}$ showed good linearity with respect to the percentage of TP+*n* contribution (Fig. 6a), which was expected. Contrary to this, the stimulation focusing was modelled and found to vary nonlinearly with σ (Fig. 6b). For all the fittings, the coefficient of determination was larger than 0.96 (Fig. S9). Note that there were some intercepts in the curves with different distances of current sinking electrodes from the centering electrode. When σ is below ~70%, pTP+1 and pTP+2 modes could deliver more focused stimulation than pTP+0 modes at the same σ, with slightly higher α for pTP+2. With σ being between 70% and 99%, pTP+1 demonstrated the most focused stimulation compared to the other pTP modes. There is only a small window, when σ is greater than 99%, for which the closest current sink to the stimulus electrode has the best focusing ability. Nevertheless, σ is a parameter of the stimulation configuration, and it would be meaningful to investigate the relationship between power consumption and stimulation focusing.

As seen in Fig. 6c, the pTP+0 modes deliver much lower $V_{SI,pp}$ at the same stimulus level, with the benefit of a slightly better focusing effect. The pTP+1 and pTP+2 modes seem to be quite similar in this regard, except that pTP+1 allows higher stimulation focusing that is comparable to that in the TP+0 mode. Though these results cannot directly prove that pTP+1 provides the best compromise between stimulation threshold and focusing for all CI recipients, they indicate some trends and compromises that should be considered when choosing various stimulation configurations. In addition, it is suggested that, beyond a certain level, increased focusing cannot be differentiated by the auditory nerve [9], so it may be worth

combining auditory nerve stimulation models with these experimental results to assess whether the TP+*n* mode can deliver improved focusing compared to other modes. It is also possible that too much current focusing might not recruit enough neurons for a reasonable comfortable loudness perception level, and current injection may need to be increased to loudness balance different stimulation types in real life before comparisons of distinguishing ability for speech or spectral patterns can be made.

It may also be interesting to culture cochlear spiral ganglion neurons in the in-vitro model, especially on the electrodes of recording wires to directly record neural excitation rates under spread stimulations.

IV. Conclusions and Future Work

We have presented a novel platform, i.e., 3D-printed unwrapped "artificial cochlea" with instrumented recording wires, to measure intracochlear current spread and compare different stimulation modes commonly investigated for cochlear implants. The results (summarized in Table S1) provided quantitative evidence of the differences in SIV distribution among MP, BP, TP stimulation modes with different configurations. Generally, there are trade-offs between the stimulation levels and focusing when comparing different stimulation modes. In addition, apical and basal current sinks can greatly affect SIV distributions in the cochlea. Moreover, we found that there is an optimum in the distance between stimulating and sinking electrodes. This platform allows customizing a 3D-printed cochlea model with cochlea geometry and electrical properties tunable to match a real cochlea, if geometry (from CT/MRI scans) and EFI (from a CI) can be available with sufficient detail, thus enabling *in-vitro* study on electrical stimulus spread for a CI user.

In future studies, we aim to investigate other advanced stimulation modes such as phased array and current steering. In addition, we envision advanced bioprinting technology will allow us to build artificial cochleae that simulate the 3D shape of human cochleae, and can be instrumented with a dense network of recording wires by microfabrication to visualize current spread distributions at a high resolution. We also wish to develop a neural model and/or to culture cochlear spiral ganglion neurons in the in-vitro model that could link the current spread distribution to how neurons respond to electrical stimuli and what CI users might hear.

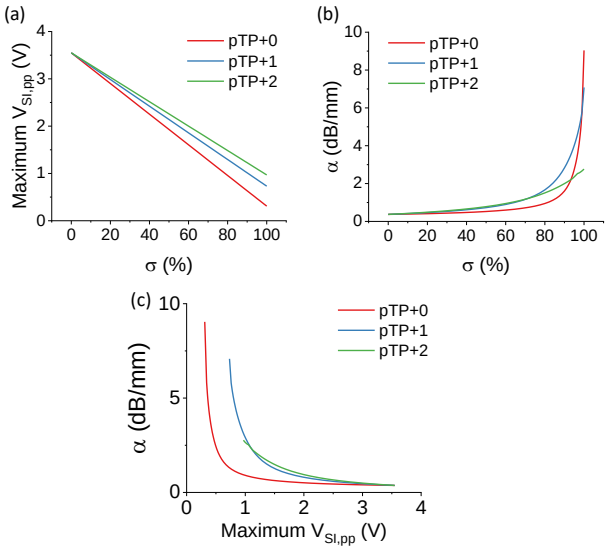

Fig. 6. (a) Modelling of the maximum peak-to-peak SIV and (b) the stimulation focusing under different pTP+*n* modes. (c) The modelled relationship between stimulation focusing and the maximum peak-to-peak SIV under different pTP+*n* modes.

References

[1] Q. J. Fu, "Temporal processing and speech recognition in cochlear implant users," *Neuroreport*, vol. 13, no. 13, pp. 1635–1639, Sep. 2002.

[2] O. Macherey and R. P. Carlyon, "Cochlear implants," *Current Biology*, vol. 24, no. 18. Cell Press, pp. R878–R884, Sep-2014.

[3] J. A. Grange, J. F. Culling, N. S. L. Harris, and S. Bergfeld, "Cochlear implant simulator with independent representation of the full spiral ganglion," *J. Acoust. Soc. Am.*, vol. 142, no. 5, pp. EL484–EL489, Nov. 2017.

[4] M. D. Fletcher, S. R. Mills, and T. Goehring, "Vibro-Tactile Enhancement of Speech Intelligibility in Multi-talker Noise for Simulated Cochlear Implant Listening," *Trends Hear.*, vol. 22, p. 2331216518797838, 2018.

[5] J. B. Firszt *et al.*, "Recognition of speech presented at soft to loud levels by adult cochlear implant recipients of three cochlear implant systems.," *Ear Hear.*, vol. 25, no. 4, pp. 375–87, Aug. 2004.

[6] F. G. Zeng *et al.*, "Development and evaluation of the Nurotron 26-electrode cochlear implant system," *Hear. Res.*, vol. 322, pp. 188–199, 2015.

[7] L. M. Friesen, R. V. Shannon, D. Baskent, and X. Wang, "Speech recognition in noise as a function of the number of spectral channels: Comparison of acoustic hearing and cochlear implants," *J. Acoust. Soc. Am.*, vol. 110, no. 2, pp. 1150–1163, Aug. 2001.

[8] Q. J. Fu and G. Nogaki, "Noise susceptibility of cochlear implant users: The role of spectral resolution and smearing," *JARO - J. Assoc. Res. Otolaryngol.*, vol. 6, no. 1, pp. 19–27, 2005.

[9] A. G. Srinivasan, D. M. Landsberger, and R. V. Shannon, "Current focusing sharpens local peaks of excitation in cochlear implant stimulation," *Hear. Res.*, vol. 270, no. 1–2, pp. 89–100, 2010.

[10] T. Goehring, J. G. Arenberg, and R. P. Carlyon, "Using Spectral Blurring to Assess Effects of Channel Interaction on Speech-in-Noise Perception with Cochlear Implants," *JARO - J. Assoc. Res. Otolaryngol.*, 2020.

[11] Q. Tang, R. Benítez, and F.-G. Zeng, "Spatial Channel Interactions in Cochlear Implants," *J. Neural Eng.*, vol. 8, no. 4, pp. 1–14, 2011.

[12] Z. Zhu, Q. Tang, F.-G. Zeng, T. Guan, and D. Ye, "Cochlear-implant spatial selectivity with monopolar, bipolar and tripolar stimulation," *Hear. Res.*, vol. 283, no. 1–2, p. 45—58, Jan. 2012.

[13] M. L. Hughes, *Objective measures in cochlear implants*. Plural Publishing, 2012.

[14] A. A. Saoji, D. M. Landsberger, M. Padilla, and L. M. Litvak, "Masking patterns for monopolar and phantom electrode stimulation in cochlear implants," *Hear. Res.*, no. 298, pp. 109–116, 2013.

[15] R. P. Carlyon, J. Monstrey, J. M. Deeks, and O. Macherey, "Evaluation of a cochlear-implant processing strategy incorporating phantom stimulation and asymmetric pulses," no. February, pp. 871–879, 2014.

[16] O. Macherey, J. M. Deeks, and R. P. Carlyon, "Extending the Limits of Place and Temporal Pitch Perception in Cochlear Implant Users," *J. Assoc. Res. Otolaryngol.*, vol. 251, pp. 233–251, 2011.

[17] V. Sankarasubramanian, J. R. Buitenweg, J. Holsheimer, and P. Veltink, "Triple leads programmed to perform as longitudinal guarded cathodes in spinal cord stimulation: A modeling study," *Neuromodulation*, vol. 14, no. 5, pp. 401–411, 2011.

[18] L. H. M. Mens, "Advances in Cochlear Implant Telemetry: Evoked Neural Responses, Electrical Field Imaging, and Technical Integrity," *Trends Amplif.*, vol. 11, no. 3, pp. 143–159, 2007.

[19] A. Kral, R. Hartmann, D. Mortazavi, and R. Klinke, "Spatial resolution of cochlear implants: The electrical field and excitation of auditory afferents," *Hear. Res.*, vol. 121, no. 1–2, pp. 11–28, Jul. 1998.

[20] F. J. Vanpoucke, A. J. Zarowski, and S. A. Peeters, "Identification of the Impedance Model of an Implanted Cochlear Prosthesis From Intracochlear Potential Measurements," *IEEE Trans. Biomed. Eng.*, vol. 51, no. 12, pp. 2174–2183, 2004.

[21] F. Vanpoucke, A. Zarowski, J. Casselman, J. Frijns, and S. Peeters, "The facial nerve canal: An important cochlear conduction path revealed by clarion electrical field imaging," *Otol. Neurotol.*, vol. 25, no. 3, pp. 282–289, May 2004.

[22] Q. Mesnildrey, O. Macherey, P. Herzog, and F. Venail, "Impedance measures for a better understanding of the electrical stimulation of the inner ear," *J. Neural Eng.*, vol. 16, no. 1, Feb. 2019.

[23] J. J. Briaire and J. H. M. Frijns, "Field patterns in a 3D tapered spiral model of the electrically stimulated cochlea," *Hear. Res.*, vol. 148, no. 1–2, pp. 18–30, Oct. 2000.

[24] F. Rattay, R. N. Leao, and H. Felix, "A model of the electrically excited human cochlear neuron. II. Influence of the three-dimensional cochlear structure on neural excitability," *Hear. Res.*, vol. 153, no. 1–2, pp. 64–79, 2001.

[25] R. K. Kalkman, J. J. Briaire, and J. H. M. Frijns, "Current focussing in cochlear implants: An analysis of neural recruitment in a computational model," *Hear. Res.*, vol. 322, pp. 89–98, 2015.

[26] T. Hanekom, "Three-dimensional spiraling finite element model of the electrically stimulated cochlea," *Ear Hear.*, vol. 22, no. 4, pp. 300–315, 2001.

[27] T. Hanekom, "Modelling encapsulation tissue around cochlear implant electrodes," *Med. Biol. Eng. Comput.*, vol. 43, no. 1, pp. 47–55, 2005.

[28] D. M. Whiten, "Electro-anatomical models of the cochlear implant," Massachusetts Institute of Technology, 2007.

[29] L. M. Litvak, A. J. Spahr, and G. Emadi, "Loudness growth observed under partially tripolar stimulation: Model and data from cochlear implant listeners," *J. Acoust. Soc. Am.*, vol. 122, no. 2, pp. 967–981, 2007.

[30] B. H. Bonham and L. M. Litvak, "Current focusing and steering: Modeling, physiology, and psychophysics," *Hear. Res.*, vol. 242, no. 1–2, pp. 141–153, 2008.

[31] J. H. Goldwyn, S. M. Bierer, and J. A. Bierer, "Modeling the electrode-neuron interface of cochlear implants: Effects of neural survival, electrode placement, and the partial tripolar configuration," *Hear. Res.*, vol. 268, no. 1–2, pp. 93–104, 2010.

[32] J. Snel-Bongers, J. J. Briaire, E. H. Van Der Veen, R. K. Kalkman, and J. H. M. Frijns, "Threshold levels of dual electrode stimulation in cochlear implants," *JARO - J. Assoc. Res. Otolaryngol.*, vol. 14, no. 5, pp. 781–790, 2013.

[33] C. C. Wu and X. Luo, "Current steering with partial tripolar stimulation mode in cochlear implants," *JARO - J. Assoc. Res. Otolaryngol.*, vol. 14, no. 2, pp. 213–231, Apr. 2013.

[34] M. Thorne, A. N. Salt, J. E. DeMott, M. M. Henson, O. W. Henson, and S. L. Gewalt, "Cochlear fluid space dimensions for six species derived from reconstructions of three-dimensional magnetic resonance images," *Laryngoscope*, vol. 109, no. 10, pp. 1661–1668, 1999.

[35] P. Tran, M. L. Richardson, and F. G. Zeng, "Input–Output Functions in Human Heads Obtained With Cochlear Implant and Transcranial Electric Stimulation," *Neuromodulation*, vol. 2019, 2019.

[36] P. Tran, A. Sue, P. Wong, Q. Li, and P. Carter, "Development of HEATHER for cochlear implant stimulation using a new modeling workflow," *IEEE Trans. Biomed. Eng.*, vol. 62, no. 2, pp. 728–735, 2015.

[37] A. B. Corporation, "Surgeon's Manual for HiFocus Helix and HiFocus 1j Electrodes," 2004.

[38] K. L. Rodenhiser and F. A. Spelman, "A Method for Determining the Driving Currents for Focused Stimulation in the Cochlea," *IEEE Trans. Biomed. Eng.*, vol. 42, no. 4, pp. 337–342, 1995.

[39] J. S. Binette, M. Garon, P. Savard, M. D. McKee, and M. D. Buschmann, "Tetrapolar measurement of electrical conductivity and thickness of articular cartilage," *J. Biomech. Eng.*, vol. 126, no. 4, pp. 475–484, Aug. 2004.

[40] S. Dovancescu, S. Saporito, I. H. F. Herold, H. H. M. Korsten, R. M. Aarts, and M. Mischi, "Monitoring thoracic fluid content using bioelectrical impedance spectroscopy and Cole modeling," *J. Electr. Bioimpedance*, vol. 8, no. 1, pp. 107–115, 2017.

[41] L. F. Lima, A. L. Vieira, H. Mukai, C. M. G. Andrade, and P. R. G. Fernandes, "Electric impedance of aqueous KCl and NaCl solutions: Salt concentration dependence on components of the equivalent electric circuit," *J. Mol. Liq.*, vol. 241, pp. 530–539, 2017.

[42] M. Bingabr, B. Espinoza-Varas, and P. C. Loizou, "Simulating the effect of spread of excitation in cochlear implants," *Hear. Res.*, vol. 241, no. 1–2, pp. 73–79, 2008.

[43] A. J. Oxenham and H. A. Kreft, "Speech perception in tones and noise via cochlear implants reveals influence of spectral resolution on temporal processing," *Trends Hear.*, vol. 18, pp. 1–14, 2014.

[44] Q. Huang, Q. Luo, Z. Chen, L. Yao, P. Fu, and Z. Lin, "The effect of electrolyte concentration on electrochemical impedance for evaluating polysulfone membranes," *Environ. Sci. Water Res. Technol.*, vol. 4, no. 8, pp. 1145–1151, 2018.

[45] R. P. Carlyon, J. M. Deeks, and O. Macherey, "Polarity effects on place pitch and loudness for three cochlear-implant designs and at different cochlear sites," *J. Acoust. Soc. Am.*, vol. 134, no. 1, pp. 503–509, Jul. 2013.

[46] O. Macherey, R. P. Carlyon, A. Van Wieringen, J. M. Deeks, and J. Wouters, "Higher sensitivity of human auditory nerve fibers to positive electrical currents," *JARO - J. Assoc. Res. Otolaryngol.*, vol. 9, no. 2, pp. 241–251, Jun. 2008.

[47] F. Rattay, "The basic mechanism for the electrical stimulation of the nervous system," *Neuroscience*, vol. 89, no. 2, pp. 335–346, Mar. 1999.

[48] O. Macherey and R. P. Carlyon, "Place-pitch manipulations with cochlear implants," *J. Acoust. Soc. Am.*, vol. 131, no. 3, pp. 2225–2236, 2012.

[49] C. N. Jolly, F. A. Spelman, and B. M. Clopton, "Quadrupolar stimulation for cochlear prostheses: Modeling and experimental data," *IEEE Trans. Biomed. Eng.*, vol. 43, no. 8, pp. 857–865, Aug. 1996.

[50] D. Strelioff, "A computer simulation of the generation and distribution of cochlear potentials," *J. Acoust. Soc. Am.*, vol. 54, no. 3, pp. 620–629, 1973.